A simplified flange-lip model for distortional buckling of cold-formed steel channel-sections with stiffened web

Huang, Xu-hao; Yang, Jian; Liu, Qing-feng; Zhu, Jue; Bai, Li; Wang, Fei-liang; Wang, Jian-hua

DOI:
10.1016/j.ijmecsci.2017.12.034

A simplified flange-lip model for distortional buckling of cold-formed steel channel-sections with stiffened web

Xu-hao Huang , Jian Yang , Qing-feng Liu , Jue Zhu , Li Bai , Fei-liang Wang , Jian-hua Wang

PII: S0020-7403(17)32869-2
DOI: 10.1016/j.ijmecsci.2017.12.034
Reference: MS 4098

To appear in: *International Journal of Mechanical Sciences*

Received date: 19 October 2017
Revised date: 28 November 2017
Accepted date: 20 December 2017

Please cite this article as: Xu-hao Huang , Jian Yang , Qing-feng Liu , Jue Zhu , Li Bai , Fei-liang Wang , Jian-hua Wang , A simplified flange-lip model for distortional buckling of cold-formed steel channel-sections with stiffened web, *International Journal of Mechanical Sciences* (2017), doi: 10.1016/j.ijmecsci.2017.12.034

Highlights

- A simplified flange-lip model is proposed to analyze the distortional buckling of CFS thin walled -section.
- The equivalent orthotropic plate model is employed to analyze the local buckling of thin walled sections.
- The simplified model can be adopted in the direct strength method (DSM).

A simplified flange-lip model for distortional buckling of cold-formed steel channel-sections with stiffened web

Xu-hao Huang[a,b] ,JianYang[a, b, c,*],Qing-feng Liu[a, b] , Jue Zhu[d], Li Bai[a,b], Fei-liang Wang[a,b] Jian-hua Wang[a, b]

[a]State Key Laboratory of Ocean Engineering, School of Naval Architecture, Ocean and Civil Engineering, Shanghai Jiao Tong University, Shanghai 200240, PR China

[b] Collaborative Innovation Center for Advanced Ship and Deep-Sea Exploration (CISSE), Shanghai 200240, P.R. China

[c] School of Civil Engineering, University of Birmingham, Birmingham B15 2TT, UK

[d] Faculty of Mechanical Engineering and Mechanics, Ningbo University, China

ABSTRACT: In the current paper presents a simplified analytical model for determining the critical stress of distortional buckling of lipped channel-sections with stiffened web made from cold-form steel (CFS). Lipped channel-section with stiffened web have been shown to have a distinct advantage in resisting local buckling and are associated with the higher distortional buckling stress, when compared to the channel-section without stiffener. It is widely used as a substitution for standard channel-section in cold form steel construction applications. In the current work, CFS channel-sections with stiffened web are investigated based on the flange-lip model. In order to determine the stiffness of rotational springs representing the restraining effect of the web to the flange–lip system, the web with different type of stiffeners is modelled as an orthopedic plate. Using the total potential energy principle, the formula for calculating the local buckling stress of the stiffened web considering loading scenarios including a pure compression and a pure bending moment are derived. The stiffness of rotational spring can be obtained. Finally , the prediction of

*) Corresponding author. E-mail addresses: j.yang.3@bham.ac.uk (J.Yang)

distortional buckling critical stress of lipped channel-section with different type of stiffened webs is carried out, which is shown to be in good agreement with those calculated by the finite strip method (FSM).

Keywords: Cold-formed steel, distortional buckling, stiffened web, analytical solution.

1. Introduction

CFS sections have been widely used in the engineering practices. In order to improve the load bearing capacity of CFS sections, without compromising the material consumption, the cross-section types tend to be more diversified and complex. Research has shown that by using web stiffeners the load bearing capacity of CFS sections can be enhanced [1]. By optimizing the shape of the CFS section, it is shown that the loading capacity of the optimized cross-sections are higher than that of standard ones such as channel- or zed-sections. Leng and Schafer [2,3] proposed several optimized cross-section of types for compression members based on finite strip method and Direct Strength Method (DSM). The results showed that with given cross-section area, those optimized sections can bear higher loading than the standard cross-section type.

In order to meet the requirement of optimization, cross-sections can be even more complicated, which makes the buckling problem of such type of section even more of concern. Many researchers have studied this problem, particularly the distortional buckling of CFS member. A simplified spring model presented in literature [4] provided an approximate solution of distortional buckling stress in lipped channel sections. In the analysis of the elastic distortional buckling of CFS section, a formula was derived by Lau and Hancock [4], which was also adopted by Australia Steel Institution [5]. Later on, this model was extended by Li and Chen [6] and Zhou et al

[7]. In addition to studying the distortional behaviour of CFS channel-section columns and beams, Li and Chen [6] developed the model for CFS sigma-section and derived the formula for predicting the critical stress of sigma-section beam by using the energy method. The stiffened plate buckling model (SPBM) presented by Zhu and Li [8], Huang and Zhu [9]. In the SPBM, the web and flange-lip were considered as an integrity. In addition to the above-mentioned works were mainly based on plate theory. Other approaches including finite strip method (FSM) [10-13], generalized beam theory (GBT) [14-17], test methods [18-21] and finite elements method (FEM) [22-25]were also adopted in the analysis of the buckling behaviour in CFS-sections.

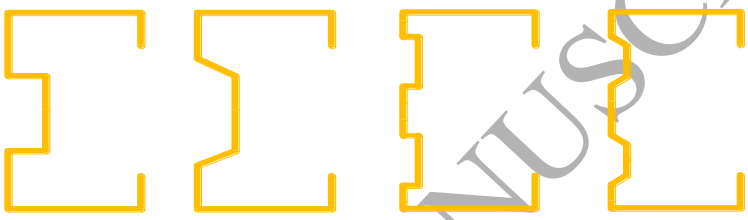

(a) Case A (b) Case B (c) Case C (d) Case D

Fig. 1. CFS channel-section with different stiffened web

In this paper, the simplified flange–lip model is employed to analyze the distortional behaviour of columns and beams with channel-sections containing different types of web stiffeners (see Fig. 1). As shown in Fig. 1, these sections that are examined in this paper are marked as “Case A”, “Case B”, “Case C” and “Case D”. In this study, the rotational spring is adopted to represent the restraining effect of the stiffened web to flange-lip. In order to determine the stiffness of rotational spring, the stiffened web is treated as an orthogonal plate with the equivalent stiffness. Based on this assumption and by using the total potential energy principle, the formula used to calculate the distortional buckling critical stress of channel-sections with the different stiffened web can be obtained. In addition, the results calculated by the finite strip method are used to validate this simplified flange-lip model. The comparison of the distortional buckling critical stress obtained by the finite strip method and those

calculated from proposed model agrees well and proves the validity of present model.

2. Flange-lip model

As is known, the different deformation characteristics between the local and distortional buckling of CFS sections is the deviation of the junction line of web and flange. The distortional buckling of CFS channel-sections is indicated by the deformation is plotted in Fig. 2a. The flange -lip can be separated from web to be used as a model for analyzing the distortional behaviour and the restraining effect provided by web to the flange–lip component can be represented by the rotational spring shown in Fig. 2b. The centroid of flange-lip (indicated as *c* in Fig. 2(b)) is defined as the origin of coordinate. The vertically axis which is parallel to lip is defined as y_c-axis. The axis which is paralleled the flange is defined as horizontal axis named z_c-axis. The displacements of the shear center in the y_c-axis and z_c-axis are indicated as *v* and *w*, respectively. Fig. 2 (b) also shows the location of the shear center, *S*, which is z_0 and y_0 away from the centroid. The rotational angel of the flange-lip section is indicated as φ.

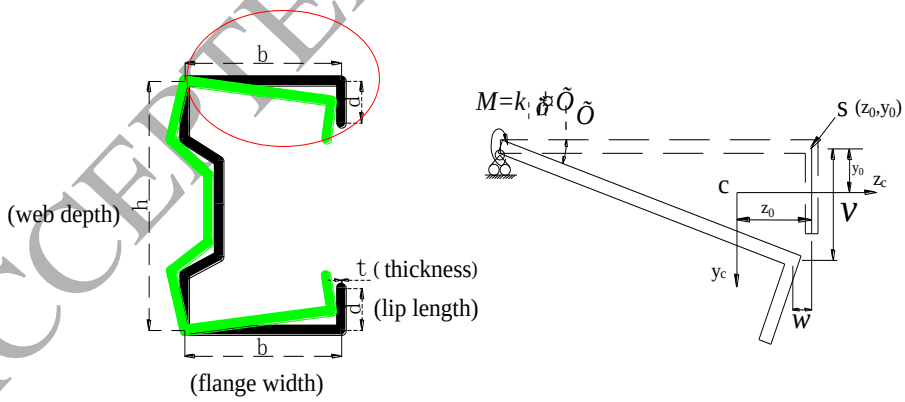

(a) (b)

Fig. 2. (a) Distortional buckling model of CFS channel-section with stiffened web; the channel-section with web depth *h*, flange width *b*, lip length *d*, and cross-section thickness *t*. (b) Flange-lip model.

The potential energy of flange-lip due to bending U_{f-l} and rotation spring U_s can be given as follows [26]:

$$U_{f-l} = \frac{1}{2}\int_0^l \left[EI_y\left(\frac{d^2w}{dx^2}\right)^2 + 2EI_{yz}\frac{d^2v}{dx^2}\frac{d^2w}{dx^2} + EI_z\left(\frac{d^2v}{dx^2}\right)^2 + GJ\left(\frac{d\varphi}{dx}\right)^2\right]dx, \quad (1)$$

$$U_s = \frac{1}{2}\int_0^l \left(k_\varphi \varphi^2\right)dx, \quad (2)$$

where l is the length of CFS channel-section members, a value of E =203 GPa is used for Young's modulus and G =78.07GPa is used for shear modulus, I_y is the inertia moment of the flange and lip about y-axis, I_z is the inertia moment of the flange and lip about z-axis, I_{yz} is the product moment of cross-section of the flange and lip, $J$is the torsional constant of cross-section of the flange and lip system, and $k_\varphi$is the effective rotational spring stiffness of the flange-lip section due to the web constraints.

The work done on the flange-lip W_{f-l} when the CFS section subjected to axial compression can be written as follow [26]:

$$W_{f-l} = \frac{\sigma_{crd}A_1}{2}\int_0^l \left[\left(\frac{dw}{dx} + y_0\frac{d\varphi}{dx}\right)^2 + \left(\frac{dv}{dx} - z_0\frac{d\varphi}{dx}\right)^2 + \left(r\frac{d\varphi}{dx}\right)^2\right]dx, \quad (3)$$

where σ_{crd} is the critical stress, $A_1 = (b+d)t$ is the cross-sectional area of the flange-lip section, $\mathrm{r} = \sqrt{\frac{I_y+I_z}{A_1}}$ is the polar radius of gyration.

The work done on the flange-lip when the CFS channel-section subjected to pure bending can be written as follow [26]:

$$W_{f-l} = \frac{\sigma_{crd}}{2}\int_0^l \left[t\left(b + d\left(1 - \frac{d}{h}\right)\right)\right]\left[\left(\frac{dw}{dx} + y_0\frac{d\varphi}{dx}\right)^2 + \left(\frac{dv}{dx} - z_0\frac{d\varphi}{dx}\right)^2 + \left(r\frac{d\varphi}{dx}\right)^2\right]dx. \quad (4)$$

The total potential energy Π of the flange -lip section, is determined as：

$$\Pi = U_{f-l} + U_s - W_{f-l} \tag{5}$$

The horizontal and vertical displacement of shear center of flange-lip section and the torsion angle can be assumed as follows:

$$w(x) = \sum_{k=1} A_k \sin\frac{k\pi x}{l}, v(x) = b\sum_{k=1} B_k \sin\frac{k\pi x}{l}, \varphi(x) = \sum_{k=1} B_k \sin\frac{k\pi x}{l}. \tag{6}$$

It is important to note that the displacement functions of shear center given in the Eq. (6) satisfy the simple supported boundary condition ($v(x) = w(x) = \varphi(x) = 0$at the position of $x = 0$ and $x = l$).

The condition of the stationary of the total potential energy leads to the condition of vanishing partial derivatives of $\Pi = U_{f-l} + U_s - W_{f-l}$ calculated with respect to the constant A_k and B_k. This requires the following conditions:

$$\frac{\partial\Pi}{\partial A_k} = \frac{\partial}{\partial A_k}\left(U_{f-l} + U_s - W_{f-l}\right) = 0, \frac{\partial\Pi}{\partial B_k} = \frac{\partial}{\partial B_k}\left(U_{f-l} + U_s - W_{f-l}\right) = 0. \tag{7}$$

Substituting Eq. (6) into Eqs. (1) - (5) and then into Eq. (7), it leads to the following 2x2 eigenvalue equation,

$$\left\{\begin{bmatrix} a_{11} & a_{12} \\ a_{21} & a_{22} \end{bmatrix} - \sigma_{crd}\begin{bmatrix} b_{11} & b_{12} \\ b_{21} & b_{22} \end{bmatrix}\right\}\begin{Bmatrix} A_k \\ B_k \end{Bmatrix} = \begin{Bmatrix} 0 \\ 0 \end{Bmatrix}. \tag{8}$$

In which,

for members subjected to axial compression,

$$a_{11} = \pi^2 EI_y, a_{12} = a_{21} = b\pi^2 EI_{yz}, a_{22} = b^2\pi^2 EI_z + GJl^2 + \frac{l^4 k_\varphi}{\pi^2}, \tag{9.a}$$

$$b_{11} = -A_1 l^2, b_{12} = b_{21} = b_{11}y_0, b_{22} = b_{11}(r^2 + (b - z_0)^2 + y_0^2). \tag{9.b}$$

for members subjected to pure bending,

$$a_{11} = \frac{\pi^2 EI_y}{l^2}, a_{12} = a_{21} = \frac{b\pi^2 EI_{yz}}{l^2}, a_{22} = \frac{GJ}{2} + \frac{b^2\pi^2 EI_z}{l^2} + \frac{l^2 k_\varphi}{\pi^2}, \tag{10.a}$$

$$b_{11} = \frac{(d^2 - (b+d)h)}{h}, b_{12} = b_{21} = b_{11}y_0, b_{22} = \frac{b_{11}(r^2 + y_0^2 + (b - z_0)^2)}{h}. \tag{10.b}$$

It is noted in the above expressions, the number of half wavelength is assumed as k=1, meaning that the length of CFS channel-section is equal to half-wavelength. The critical stress σ_{crd} in Eq. (8) can be written as follow,

$$\sigma_{crd} = \frac{(a_{11}b_{22}+a_{22}b_{11}-2a_{12}b_{12}) \pm \sqrt{(2a_{12}b_{12}-a_{11}b_{22}-a_{22}b_{11})^2-4(a_{11}a_{22}-a_{12}^2)(b_{11}b_{22}-b_{12}^2)}}{2(b_{11}b_{22}-b_{12}^2)t}$$

3. Local buckling of stiffened web subjected to axial compression or pure bending

In the prediction of the elastic buckling stress of a simple supported plate, a formula has been derived by Timoshenko [27] based on the thin plate theory. The estimation of critical local buckling stress of the stiffened web is an essential part of this process, providing the access for calculating the rotational spring stiffness which considers the restraint of web by modifying the rotating restraint stiffness of web connecting with the flange-lip (see Fig. 2b). With the presence of web stiffener, this formula for the flat plate can not be used directly, which has led to the necessity of calculating the critical buckling stress of plate with stiffeners.

The buckling analysis of the stiffened plate (see Fig. 3) usually bases on the assumption that the plate is anisotropic with the equivalent bending stiffness. Analytical approaches have been proposed to predict the critical local buckling stress of stiffened plates, by considering the stiffened plate as an orthopedic plate [28]. Easley and Mofarland [29] also presented the equivalent assumption to analyze the buckling of corrugated plate and derived the formulae for calculating the equivalent flexural stiffness.

In this paper, equivalent assumption is adopted, i.e. treating the stiffened web as an orthotropic rectangle plate with uniform thickness. To create a coordinate system whose *x*- and *y*- axis are set along the longitudinal and vertical directions of the web

plane respectively (see Fig. 3). Therefore, the buckling problem of stiffened web can be analyzed by classical plate theory. Finally, based on the equivalent assumption, the formula for calculating critical stress of web with sitffener can be derived by using total potential energy principle.

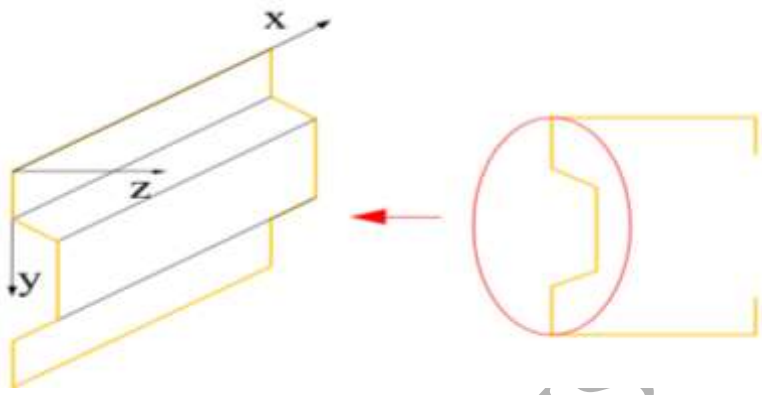

Fig. 3 Coordinate system of stiffened web

According to the classical plate theory, the strain energy of stiffened-web can be written as follow:

$$U_p = \frac{1}{2}\int_0^l \int_0^h \left[\left(v_y D_x + v_x D_y\right)\left(\frac{\partial^2 w_p}{\partial^2 x}\frac{\partial^2 w_p}{\partial^2 y}\right) + D_x\left(\frac{\partial^2 w_p}{\partial^2 x}\right)^2 + D_y\left(\frac{\partial^2 w_p}{\partial^2 y}\right)^2 + 4D_{xy}\left(\frac{\partial^2 w_p}{\partial x \partial y}\right)^2\right] dy dx \quad (12)$$

where: D_x and D_y are the flexural rigidities of stiffened web in the *x*- and *y*-directions, respectively, D_{xy} denotes the torsional stiffness, a value of $v_x = v_y = v = 0.3$ is used for Poisson's ratio of stiffened web in the *x*- and *y*- directions, respectively, and w_p represents the displacement function of stiffened web.

The work done on the stiffened web can be given as follows:

for members subjected to axial compression,

$$W_P = \frac{1}{2} t \sigma_{crw} \int_0^l \int_0^h \left(\frac{\partial w_p}{\partial x}\right)^2 dy\, dx, \quad (13)$$

where σ_{crw} is the buckling critical stress of stiffened web plate,

for members subjected to pure bending,

$$W_P = \frac{1}{2} t\sigma_{crw} \int_0^l \int_0^h \left(1 - \frac{2y}{h}\right) \left(\frac{\partial w_p}{\partial x}\right)^2 dy\, dx, \quad (14)$$

The total potential energy of stiffened web Π_p can be given as follow:

$$\Pi_p = U_p - W_p. \quad (15)$$

The displacement function of stiffened web with the simple-support can be assumed as follow:

$$w_p = \sum_{mn} A_{mn} \sin\left(\frac{m\pi x}{l}\right) \sin\left(\frac{n\pi x}{h}\right), \quad (16)$$

for members subjected to axial compression (m =1; n =1,),

$$w_p = A_{11} \sin\left(\frac{\pi x}{l}\right) \sin\left(\frac{\pi y}{h}\right), \quad (17.a)$$

for members subjected to pure bending (m =1; n =1, 2),

$$w_p = A_{11} \sin\left(\frac{\pi x}{l}\right) \sin\left(\frac{\pi y}{h}\right) + A_{12} \sin\left(\frac{\pi x}{l}\right) \sin\left(\frac{2\pi y}{h}\right), \quad (17.b)$$

where A_{mn} (m = 1, 2….; n = 1, 2…) is coefficient, m is the number of half-wavelength along the x-axial. l represents the length of the channel-section, and the formulae for l are obtained in section 5. Note that the length of plate is equal to the half-wave length, when m =1.

The condition when the buckling occurs is the total potential of the system to have a stationary condition with respect to the coefficient A_{mn}:

$$\frac{\partial \Pi_P}{\partial A_{11}} = \frac{\partial}{\partial A_{11}} \left(U_p - W_p\right) = 0, \quad (18)$$

substituting Eqs. (12,13, 17.a) into Eq. (18), it leads to the formula for calculating the critical stress of stiffened web under axial compression:

$$\sigma_{crw,l=l_{cr}} = \left(\frac{h\pi^4 D_x}{4l_{cr}^3} + \frac{\pi^4 D_{xy}}{h l_{cr}} + \frac{l_{cr}\pi^4 D_y}{4h^3} + \frac{\pi^4 \left(D_y v_x + D_x v_y\right)}{4h l_{cr}}\right) \times \frac{4l_{cr}}{h\pi^2 t}. \quad (19)$$

Then, the critical stress of stiffened web under pure bending is obtained by substituting Eqs. (12, 14 and 17.b) into Eq. (18) and yields

$$\frac{\partial \Pi}{\partial A_{11}} = \frac{\partial}{\partial A_{11}}(U_P - W_P) = 0, \frac{\partial \Pi}{\partial A_{12}} = \frac{\partial}{\partial A_{12}}(U_P - W_P) = 0, \tag{20}$$

$$\left\{\begin{bmatrix} a_{11} \\ a_{12} \end{bmatrix} - \sigma_{crw}\begin{bmatrix} b_{11} \\ b_{12} \end{bmatrix}\right\}\begin{Bmatrix} A_{11} \\ A_{12} \end{Bmatrix} = \begin{Bmatrix} 0 \\ 0 \end{Bmatrix}, \tag{21.a}$$

$$\sigma_{crw,l=l_{cr}} = \sqrt{\frac{a_{11}b_{12}}{a_{12}b_{11}}}, \tag{21.b}$$

in which

$$a_{11} = \left(\frac{hD_x}{4l_{cr}^2} + \frac{l_{cr}^2 D_y}{4h^3} + \frac{D_y v_x + D_x v_y + 4D_{xy}}{4h}\right), \tag{22.a}$$

$$a_{12} = b_{11} = \frac{8ht\sigma_{crw}}{9\pi^4}, \tag{22.b}$$

$$b_{12} = \left(\frac{hD_x}{4l_{cr}^2} + \frac{4l_{cr}^2 D_y}{h^3} + \frac{D_y v_x + D_x v_y + 4D_{xy}}{4h}\right), \tag{22.c}$$

The dimensions of stiffened web plate are shown in Fig. 4. For the Case A and Case C, the angle of stiffener is $\theta = 90^\circ$. Whereas for the Case B and Case D, the angle of stiffener is $\theta < 90^\circ$.The CFS section with stiffened-web (Case A and Case B) are known as sigma-section. The equivalent flexural and torsional stiffness of stiffened web (see Fig. 4) can be estimated as follows [29]:

$$D_x = \frac{h}{s}\frac{Et^3}{12}, D_y = \frac{EI_{yw}}{h}, D_{xy} = \frac{Est^3}{6h(1+v)}, \tag{23.a}$$

$$I_{yw} = 2\left(h_w t\frac{h_s^2}{4} + \frac{h_w t^3}{12} + \frac{(h_s/\sin\theta)^3 t}{12}\sin^2\theta\right), \tag{23.b}$$

for Case A and Case B:

$$s = 2h_{ow} + 2(h_s/\sin\theta) + h_w, \tag{24.a}$$

for Case C and Case D:

$$s = 2h_{ow} + 4(h_s/\sin\theta) + 2h_w + h_{mw}, \tag{24.b}$$

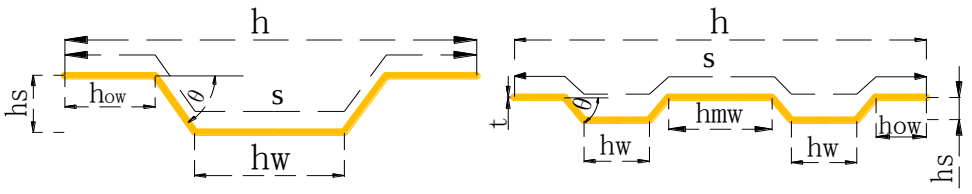

(a)Cases A ($\theta = 90^{\circ}$) and Case B ($\theta < 90^{\circ}$)) (b) Cases C ($\theta = 90^{\circ}$) and Case D ($\theta < 90^{\circ}$)

Fig. 4 Dimension of web with different stiffeners； h_w and h_s represent the height and width of the stiffener, respectively, h_{ow} is the outer web, and s is the full-length of stiffened web.

4. Determination of rotation spring stiffness in channel-section with stiffened web

The rotational spring shown in Fig 2b represents the effect of the web's restraint to the rotation of the flange-lip section. The value of the rotational spring stiffness can be considered by introducing a reduction factor of critical stress of web plate which is assumed as a simply supported plate, as observed by Lau and Hancock [4]. The rotational spring stiffness of Lau and Hancock model is extended by Li and Chen [6] by considering the influence of the local buckling. Zhou et al [7] also presented the formulae to calculate the value of the rotational spring by introducing the reduction factor to take into account the web bending. Ajeesh and Jayachandran [30] proposed an empirical expression for the rotational stiffness, k_{φ}, by comparing the results calculated from the proposed formula with those from finite strip results. Furthermore, Zhao et al [31] proposed the hand calculation method to determine the rotational stiffness due to at the sheeting-purlin connection. In this study, based on the Li [6] and Zhou [7] model, the rotational spring coefficient considering the effect of different web stiffeners is presented.

The rotational spring coefficient of CFS section members subjected axial compression can be defined as follows:

for Case A and Case B,

$$k_\varphi = \frac{2D\alpha}{h}\left(1 - \frac{\sigma^*_{crd}}{\sigma_{crw}}\right), \quad (25.a)$$

$$\alpha = \frac{b(0.03h_s + 0.32 + 0.1\cos\theta)}{d(1+2h/b)}, \quad (25.b)$$

where α is the regression model of extensive parametric analysis using the Finite Strip Method (FSM).

The rotational spring coefficient of CFS channel-section members subjected pure bending can be defined as follows:

for Case A and Case B,

$$k_\varphi = \frac{(1+0.006h_s)4D}{h}\left(1 - \frac{\sigma^*_{crd}}{\sigma_{crw}}\frac{h}{h+z_0}\right), \quad (26)$$

for Case C and Case D,

$$k_\varphi = \frac{(1+0.02h_s)4D}{h}\left(1 - \frac{\sigma^*_{crd}}{\sigma_{crw}}\frac{h}{h+z_0}\right), \quad (27)$$

where, σ_{crw} is the buckling stress of the web of a member subjected to compression or pure bending defined by Eqs. (19), (21.b), σ^*_{crd} can be defined in Eq. (11) with $k_\varphi = 0$.

5. Comparison of the present model with finite strip method

According to the investigated example, stiffeners provides an effective way of enhancing the local buckling resistance of CFS channel-section and achieving higher efficiency in the cross-sectional resistance. The comparison of the critical stress is made between the CFS channel-section with stiffened web and without stiffener analyzed by CUFSM [32]. By observing the buckling curves showed in Figs.5 and 6, it is easy to see that the critical stresses of local and distortional buckling of channel-sections with stiffened web are higher than those of channel-section without stiffener under axial compression or pure bending.

The half wavelength-buckling stress curves of CFS channel-section member which are subjected to axial compression and pure bending are respectively shown in

Figs. 5. Under the axial compression, the buckling half-wavelength of CFS channel -section with the stiffened web is longer than those of CFS section without stiffener (see Fig 5(a)). Formula have been presented for calculating the half-wavelength of CFS section with stiffened web based on the channel-section without stiffener, namely,

$l_{cr} = (1 + 0.15h/b)4.8\left(\frac{I_y b^2 h}{t^3}\right)^{0.25}$. It can be applied to approximately estimate the half-wavelength of the buckling mode of CFS channel-section columns with stiffened webs when the height of web is greater than the width of flange. Similar to α in Eq. (25b), l_{cr} is obtained by performing regression analysis based on the extensive parametric analysis by FSM (see Fig 6). It is found that a 20% error from the calculation results for the half-wavelength produces only a maximum of 7% error in the critical stress [4]. Then half-wavelength can be obtained from the above formula. For the beams with the stiffened web, the stiffener has negative effect on the half-wavelength (see Fig 5(b)). Therefore, the half-wavelength of CFS channel-section beams with the stiffened web can be defined by$l_{cr} = 4.8\left(\frac{I_y b^2 h}{t^3}\right)^{0.25}$.

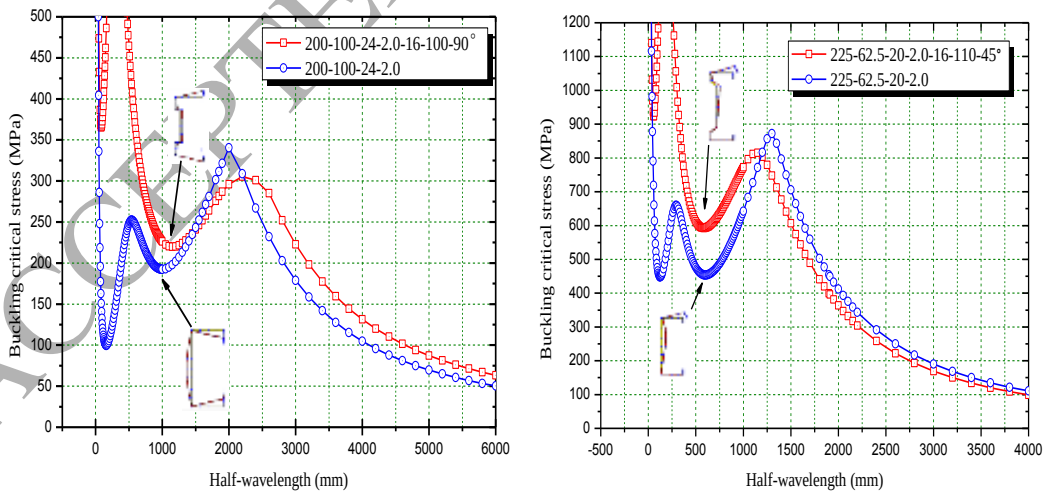

(a) (b)

Fig. 5. Comparison of the critical stresses between the CFS channel-section with stiffened web and without stiffener. (a) For members under axial compression

(*h*-*b*-*d*-*t*-h_s-h_w-θ: 200-100-24-2.0-16-100-90°; unit: mm); (b) For members under pure bending (*h*-*b*-*d*-*t*-h_s-h_w-θ: 225-62.5-20-2.0-16-110-45°, unit: mm).

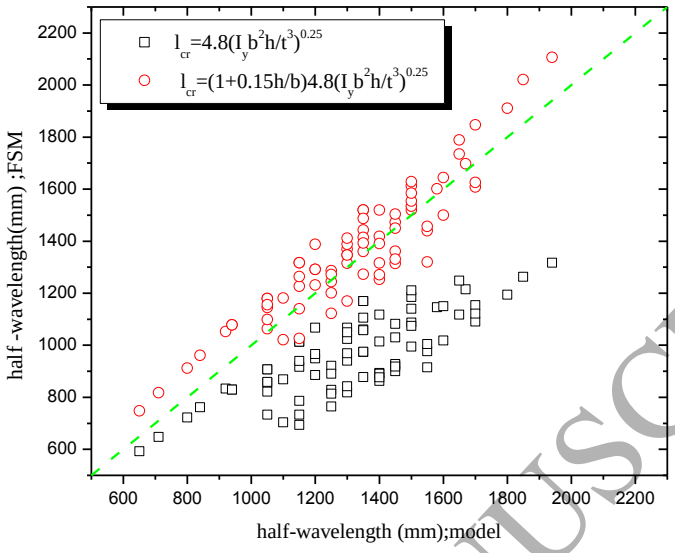

Fig. 6. Comparisons of half-wavelengths of channel sections with stiffened web between the formulae and FSM.

The formula $l_{cr} = 4.8\left(\frac{I_y b^2 h}{t^3}\right)^{0.25}$ used to estimate the half-wavelength of CFS channel- and Z-section without stiffener is developed by Lau and Hancock[4]. The formula $l_{cr} = (1 + 0.15h/b)4.8\left(\frac{I_y b^2 h}{t^3}\right)^{0.25}$ is used to estimate the half-wavelength of CFS channel-section with stiffened web. The channel-sections with different height/width ratio (h/b) show in Table 1 and Table 2 are selected as example.

5.1 Simplified flange-lip model for CFS channel-section with stiffened web under axial compression

Comparing the buckling curves between the channel- and sigma-section subjected axial compression, Li and Chen [6] indicated that for CFS sigma-section columns with a narrow flange, the distortional buckling mode may not triggered. For axial

compression channel-section column (Case C and Case D) , the buckling curves plotted in Fig. 7, where only local and lateral torsional bucking are observed. In this paper, for channel-section members subjected to axial compression, we will focus on the range of sections that will experience the distortional buckling, e.g. Case A and Case B. Cases C and Cases D are not particularly considered.

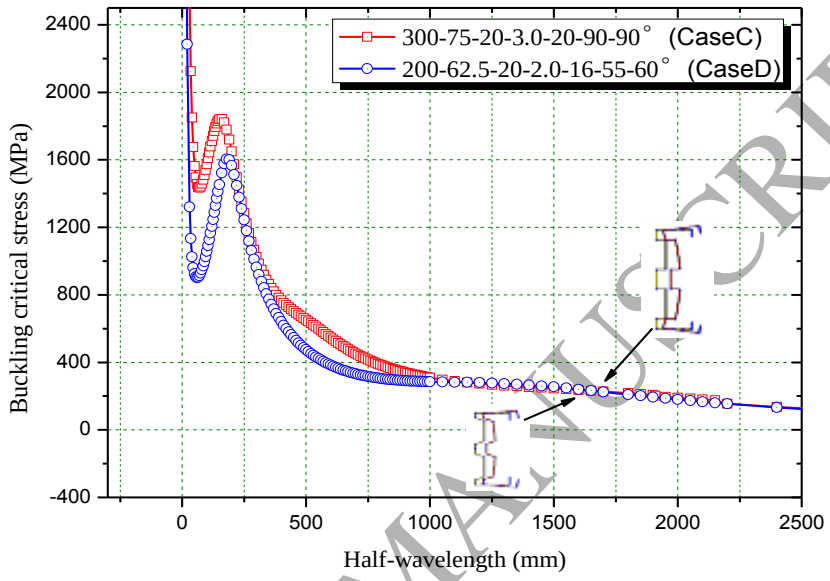

Fig. 7. Buckling curves of CFS channel-section with stiffened web under axial compression (Case C and Case D) (h-b-d-t-h_s-h_w-θ: 200-62.5-20-2.0-16-55-60°or 300-75-20-3.0-20-90-90°, unit: mm)

The results calculated by the finite strip method (FSM) have been used to demonstrate the validity of the simplified flange-lip model proposed above. The dimensions of CFS channel-section with stiffened web are shown in Tables 1 and 2. The critical stresses of Case A with the stiffener widths of 16 mm and 20 mm are given in Table 1. Meanwhile, Table 2 also reports critical stresses for Case B(θ =45) with the stiffener widths of $h_s = 16mm$ and $h_s = 20mm$. The comparisons results between the presented model and FSM are plotted in Fig 8. For the proposed model, the mean value and standard deviation of $\sigma_{crd,model}/\sigma_{crd,FSM}$ are 1.004 and 0.036, respectively. By observing the results presented in Fig 8, it can be seen that the

proposed flange-lip model can be used to accurately predict the distortional buckling critical stress for Case A and Case B.

Table1 Distortional buckling critical stresses of channel-section using FSM and the presented model (Case A:$h_s = 16mm, \theta = 90^{\circ}$; $h_s = 20mm, \theta = 90^{\circ}$.)

Section dimensions, mm	Thickness mm	$\sigma_{crd,FSM}$ (hs =16) MPa	$\sigma_{crd,model}$ (hs =16) MPa	$\sigma_{crd,FSM}$ (hs=20) MPa	$\sigma_{crd,model}$ (hs=20) MPa
h=200	1.5	160.47	164.25	176.65	181.59
b=100	1.8	195.72	199.61	215.02	220.48
d=24	2.0	219.74	223.70	241.17	246.92
h_w=110	2.5	282.09	285.81	308.53	314.90
	3.0	347.21	350.74	378.75	385.67
h=225	1.5	149.12	144.09	168.48	160.06
b=100	1.6	159.20	154.46	180.56	171.52
d=20	1.8	181.10	175.50	205.05	194.78
h_w=115	2.0	203.44	196.98	229.96	218.47
	3.3	237.81	230.03	268.14	254.86
	2.5	262.42	252.64	294.13	279.69
h=240	1.6	154.99	150.56	173.11	166.78
b=100	1.8	176.05	170.91	196.33	189.19
d=24	2.0	197.58	191.63	219.89	211.98
h_w=110	2.5	252.88	245.20	280.33	270.68
	3.0	310.64	301.38	342.94	331.95
h=265	1.6	143.28	139.04	158.09	154.17
b=100	1.8	162.93	157.90	179.11	174.97
d=24	2.0	182.73	177.12	200.41	196.14
h_w=135	2.3	213.07	206.65	232.88	228.60
	2.5	235.51	221.66	254.87	245.93
	2.8	265.34	257.84	292.44	284.64
h=300	2.0	157.48	147.88	175.91	173.70
b=105	2.3	183.49	172.71	204.64	202.40
d=24	2.5	201.19	189.70	223.85	221.95
h_w=150	2.8	228.19	215.85	253.09	251.92
	3.0	246.71	233.74	272.86	272.35

Table 2 Distortional buckling critical stresses of channel-section using FSM and the presented model (Case B: $h_s = 16mm, \theta = 45^\circ$; $h_s = 20mm, \theta = 45^\circ$.)

Section dimensions, mm	Thickness mm	FSM (hs=16) MPa	Present model(hs=16) MPa	FSM (hs=20) MPa	Present model(hs=20) MPa
h=140	1.5	244.72	248.46	264.99	272.64
b=80	1.8	298.91	302.36	323.17	333.55
d=20	2.0	336.02	339.17	362.92	373.85
h_w=50	2.5	432.24	434.39	465.76	477.78
	3.0	533.43	534.38	573.45	586.45
h=200	1.5	166.38	173.69	180.82	191.12
b=100	1.8	202.96	210.89	220.21	231.87
d=24	2.0	227.96	236.21	247.08	259.54
h_w=100	2.5	292.64	301.38	315.64	330.61
	3.0	360.44	369.36	388.96	404.46
h=230	1.5	152.00	154.53	168.38	170.24
b=100	1.8	185.35	187.77	204.9	206.70
d=24	2.0	208.13	210.40	229.83	231.49
h_w=120	2.5	267.02	268.76	293.94	295.22
	3.0	328.69	329.76	360.76	361.57
h=260	1.5	134.63	139.88	149.5	154.27
b=100	1.8	164.13	170.08	181.86	187.46
d=24	2.0	184.28	190.67	203.94	210.05
h_w=150	2.5	236.33	243.81	260	268.21
	3.0	290.79	299.43	319.59	328.84
h=300	1.8	138.47	148.05	155.68	163.70
b=100	2.0	155.39	165.94	174.39	183.41
d=24	2.3	181.35	193.38	205.49	213.59
h_w=170	2.5	199.03	212.09	224.96	234.13
	2.8	226.15	240.80	254.70	265.59
	3.0	244.61	260.39	274.79	287.00

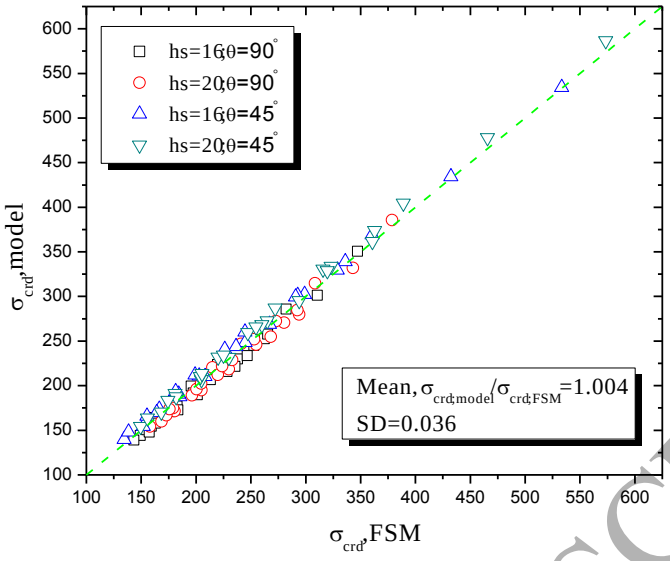

Fig 8. Comparisons of critical stresses of CFS columns (Case A and Case B). The calculated results of the proposed model and FSM are listed in Table 1 and Table 2.

5.2 The simplified flange-lip model for CFS channel-section with stiffened web under pure bending

Under the pure bending, the distortional buckling mode of CFS channel-section with stiffened web often appears. The CFS channel-section beams of Case A and Case B which are produced by a UK manufacturer Albion [33] are employed in the verification. The geometric parameters of Albion CFS sections are cited in Table 3. The dimensionless stresses of the comparison are performed in Figs. 9 to 11. It is worth-noting that, the height of stiffener (h_s) h_s =16mm and h_s =20mm are considered. The angle of stiffener (θ) is varied as 45º, 60º, and 90º.. In Figs.9-11, the vertical and horizontal axes in the figures stand for $\sigma_{crd,m}/\sigma_y$ and $\sigma_{crd,FSM}/\sigma_y$,respectively.

Fig.9 shows the distortional buckling critical stresses of Case A calculated by the FSM and the flange-lip model. It can be found that the critical stresses derived by the flange- lip model agree well with those obtained from FSM. For the Case B, Figs. 10 and 11 represent the values of $\sigma_{crd,m}/\sigma_y$ vs. that of $\sigma_{crd,FSM}/\sigma_y$ of the channel-section beams subjected to the pure bending. Fig. 10 is for the channel-section beam with

$\theta = 60^{\circ}$; whereas Fig. 11 is for CFS beam with stiffener width of h_s=16mm, 20mm and the angel of stiffener $\theta = 45^{\circ}$. It can be found that the analyzed modeling results and numerical results (FSM) are in a good agreement.

Table 3 Dimensions of CFS channel-sections (Case A & Case B) (unit: mm)

Section code	Web depth, h	Flange width, b	Lip length, d	Outer web, h_{ow}	Thickness, t	Case A & Case B
ASB200	200	62.5	20	45	1.2,1.3,1.4,1.5,1.6,1.8,2.0,2.3,2.5	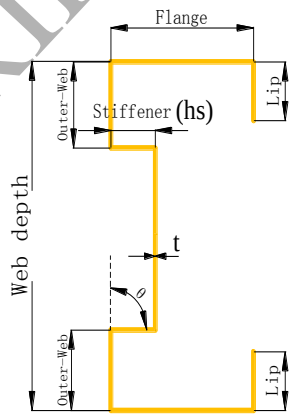
ASB225	225	62.5	20	45	1.2,1.3,1.4,1.5,1.6,1.8,2.0,2.3,2.5	
ASB240	240	62.5	20	50	1.5,1.6,1.8,2.0,2.3,2.5,2.8	
ASB265	265	62.5	20	60	1.5,1.6,1.8,2.0,2.3,2.5,2.8	
ASB300	300	75	20	60	1.8,2.0,2.3,2.5,2.8,3.0	

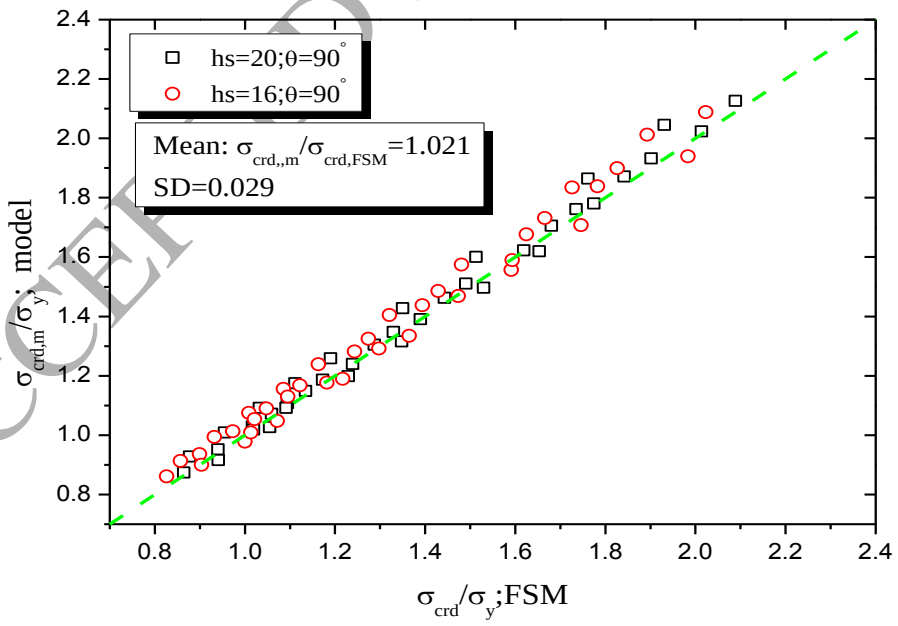

Fig. 9. Comparison of critical stresses of channel-section beams with stiffened web (Case A, $\theta = 90^{\circ}$) between the proposed model and FSM.

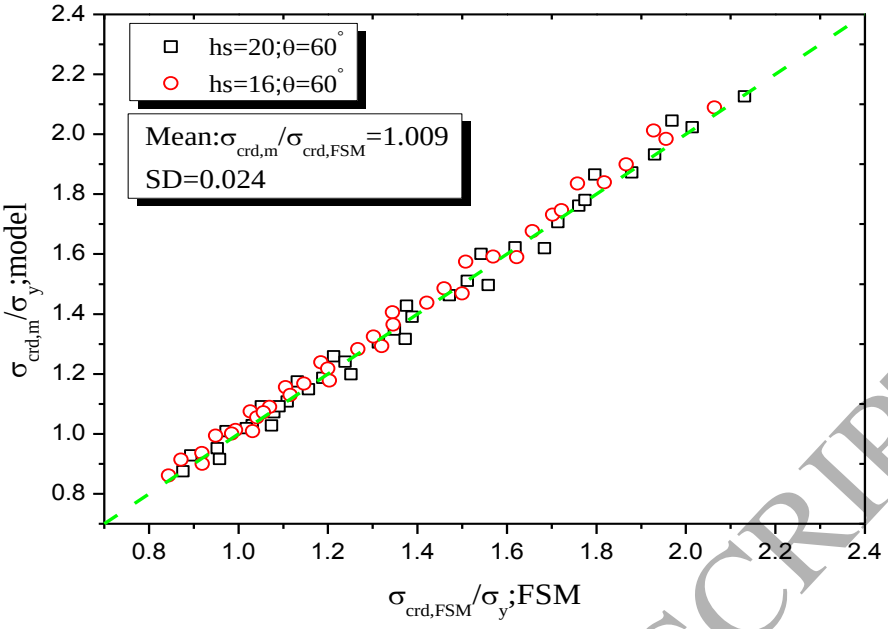

Fig. 10. Comparison of critical stresses of channel-section beams with stiffened web (Case B, $\theta = 60^{\circ}$) between the proposed model and FSM.

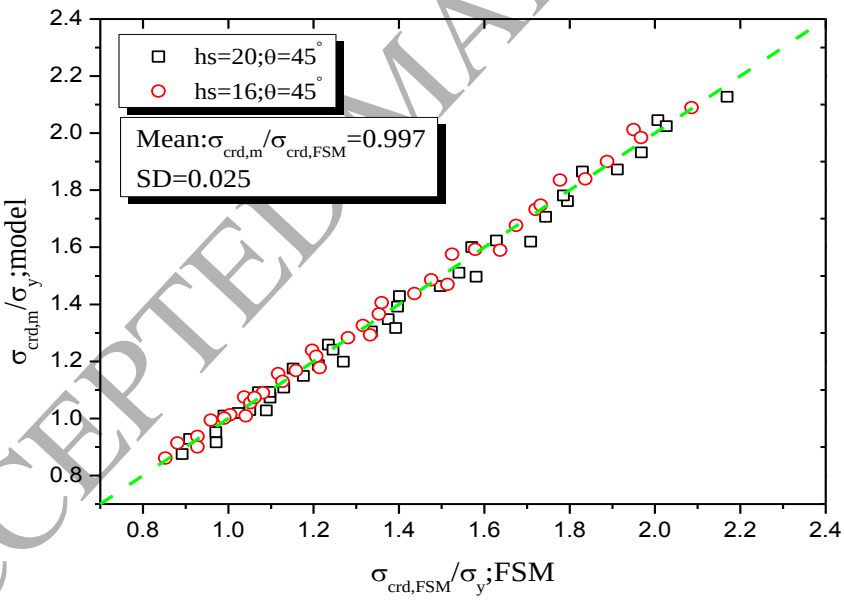

Fig. 11. Comparison of critical stresses of channel-section beams with stiffened web (Case B, $\theta = 45^{\circ}$) between the proposed model and FSM.

The details of geometric parameters of CFS channel-sections with stiffened web (Case C and Case D) are listed in Table 4. Fig. 12 compares the dimensionless of critical stresses of CFS channel-section with different stiffener width (h_s=16mm and

h_s =20mm) with the same value of angle $\theta = 90^{\circ}$. The average value of $\sigma_{crd,m}/\sigma_{crd,FSM}$ is 1.003 and standard deviation is 0.035.

For Case D, the CFS channel-sections with stiffener width of h_s=16mm, 20mm and angle of $\theta = 60^{\circ}, \theta = 75^{\circ}$ are considered in the current investigation. Figs. 13-14 report the ratio of critical stress to yield stress from both methods. For Case D with the angle of $\theta = 75^{\circ}$, the average value of $\sigma_{crd,m}/\sigma_{crd,FSM}$ and standard deviation are 0.991 and 0.034, respectively(see Fig. 13). For Case D with the angle of $\theta = 60^{\circ}$, the average value of $\sigma_{crd,model}/\sigma_{crd,FSM}$ and standard deviation are 0.985 and 0.035,respectively. As revealed in Figs. 13-14, a good agreement is found between the flange-lip model and finite strip method (FSM).

Table 4 Dimensions of CFS channel-sections (Case C & Case D) (unit: mm)

Section code	h	b	*d*	h_w	hr	*t*	Case C & Case D
ADSB200	200	62.5	20	55	16,20	1.2,1.3,1.4,1.5,1.6,1.8,2.0,2.3,2.5	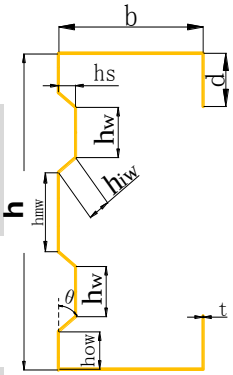
ADSB225	225	62.5	20	65	16,20	1.2,1.3,1.4,1.5,1.6,1.8,2.0,2.3,2.5	
ADSB240	240	62.5	20	70	16,20	1.5,1.6,1.8,2.0,2.3,2.5,2.8	
ADSB265	265	62.5	20	80	16,20	1.5,1.6,1.8,2.0,2.3,2.5,2.8	
ADSB300	300	75	20	90	16,20	1.8,2.0,2.3,2.5,2.8,3.0	

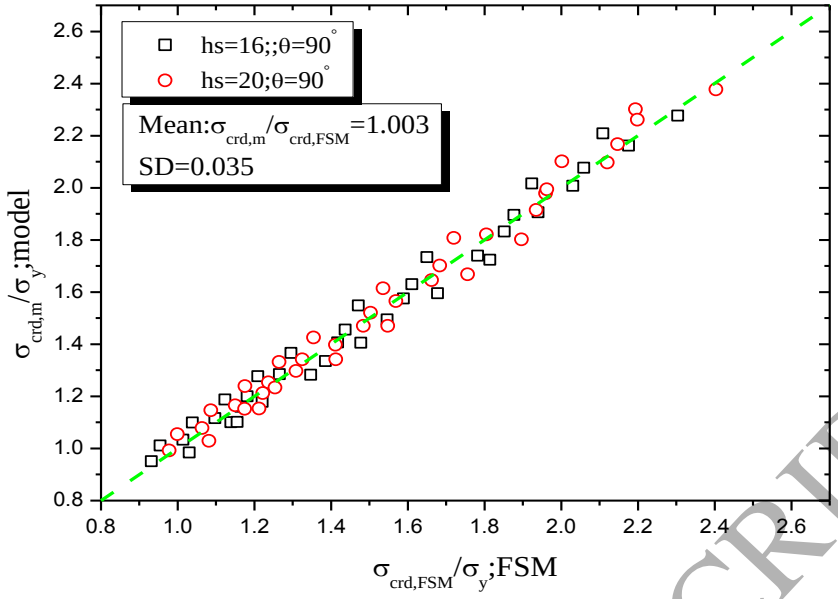

Fig. 12 Comparison of critical stresses of channel-section beams with stiffened web (Case C: $\theta = 90^{\circ}$) between the proposed model and FSM.

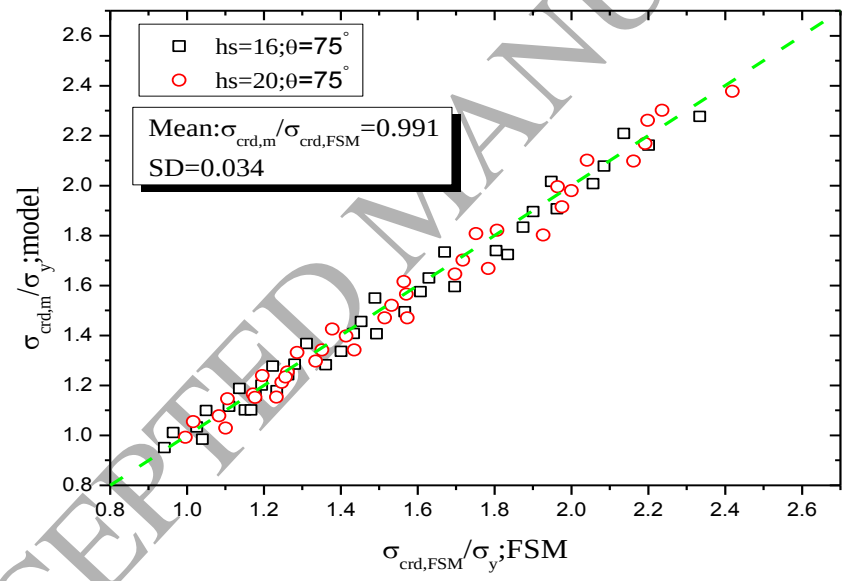

Fig. 13 Comparison of critical stresses of channel-section beams with stiffened web (Case D: $\theta = 75^{\circ}$) between the proposed model and FSM.

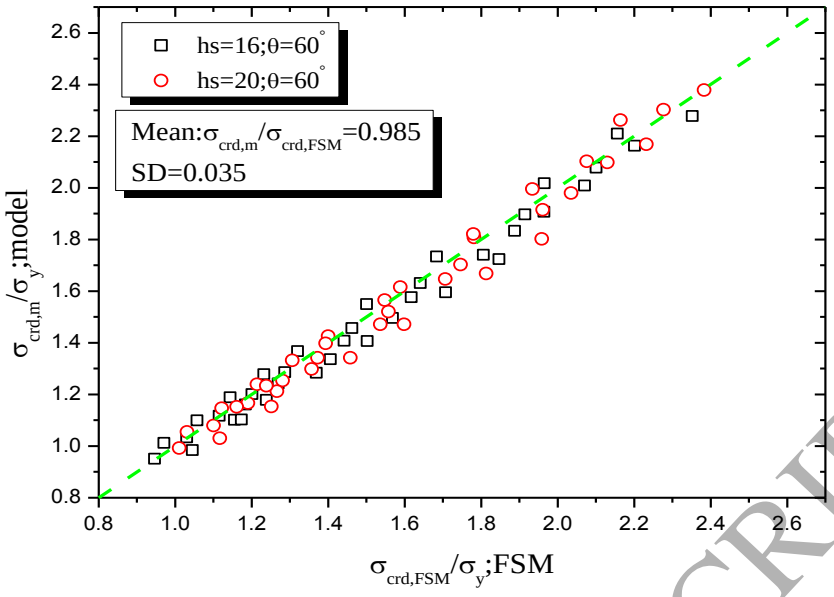

Fig. 14 Comparison of critical stresses of channel-section beams with stiffened web (Case D: $\theta = 60^{\circ}$) between the proposed model and FSM.

6. Conclusions

The distortional buckling behaviour of CFS section with stiffened webs subjected to axial compression or pure bending is investigated in this paper. The analytical model for calculating the critical stress of the web plate with different stiffener is proposed by assuming it as the orthotropic plate. Based on that, the formulae for calculating the rotational spring stiffness is derived. A design-oriented analytical formulae for predicting the distortional buckling critical stress of CFS section with different stiffened webs are developed based on the principle of minimum potential energy. In order to validate the proposed model, the analyzed results are compared with the numerical examples calculated by finite strip method. Excellent agreement can be observed indicating the high accuracy of the proposed model in this paper. The model can be easily used in the engineering design using simple spread sheet.

Acknowledgements

The authors acknowledge the financial supports received from National Key Research and Development Program of China [Grant No. 2017YFC0806103], Science Research Plan of Shanghai Municipal Science and Technology Committee [Grant No. 17DZ1200306], National Natural Science Foundation of China (No. 51378308, 11572162).

References:

[1] Shifferaw Y, Schafer BW. Cold-formed steel lipped and plain angle columns with fixed ends. Thin-Walled Structures. 2014;80：142-52.

[2] Leng J, Guest JK, Schafer BW. Shape optimization of cold-formed steel columns. Thin-Walled Structures. 2011;49(12)：1492-503.

[3] Leng J, Li Z, Guest JK, Schafer BW. Shape optimization of cold-formed steel columns with fabrication and geometric end-use constraints. Thin-Walled Structures. 2014;85：271-90.

[4] Lau CW, Hancock GJ. Distortional buckling formulas for channel columns. Journal of Structural Engineering. 1987;133(5)：1063-78.

[5] Standard Australia, Cold-formed steel structures AS/NZS 4600: Sydney (NSW. Australia). 2005.

[6] Li LY, Chen JK. An analytical model for analysing distortional buckling of cold-formed steel sections. Thin-Walled Structures. 2008;46(12)：1430-6.

[7] Zhou XH, Liu ZK, He ZQ. General distortional buckling formulae for both fixed-ended and pinned-ended C-section columns. Thin-Walled Structures. 2015;94：603-11.

[8] Zhu J, Li LY. A stiffened plate buckling model for calculating critical stress of distortional buckling of CFS beams. International Journal of Mechanical Sciences. 2016;115–116：457-64.

[9] Huang XH, Zhu J. A stiffened-plate buckling model for calculating critical stress of distortional buckling of CFS columns. International Journal of Mechanical Sciences. 2016;119：237-42.

[10] Lau SCW, Hancock GJ. Buckling of thin flat-walled structures by a spline finite strip method. Thin-Walled Structures. 1986;4(4)：269-94.

[11] Schafer BW, Li Z, Moen CD. Computational modeling of cold-formed steel. Thin-Walled Structures. 2010;48(10-11)：752-62.

[12] Chu XT, Ye ZM, Li LY, Kettle R. Local and distortional buckling of cold-formed zed-section beams under uniformly distributed transverse loads. International Journal of Mechanical Sciences. 2006;48(4)：378-88.

[13] Yuan WB, Cheng SS, Li LY, Kim B. Web-flange distortional buckling of partially restrained cold-formed steel purlins under uplift loading. International Journal of Mechanical Sciences. 2014;89：476-81.

[14] Davies JM, Leach P. First-order generalised beam theory. Journal of Constructional Steel Research. 1994;31(2-3)：187-220.

[15] Davies JM, Leach P, Heinz D. Second-order generalised beam theory. Journal of Constructional Steel Research. 1994;31((2-3)).

[16] Silvestre N, Camotim D. Distortional buckling formulae for cold-formed steel C- and Z-section members : Part II—Validation and application. Thin-Walled Structures. 2004;42(11)：1599-629.

[17] Garcea G, Gonçalves R, Bilotta A, Manta D, Bebiano R, Leonetti L, et al. Deformation modes of thin-walled members: A comparison between the method of Generalized Eigenvectors and Generalized Beam Theory. Thin-Walled Structures. 2016;100：192-212.

[18] Casafont M, Magdalena Pastor M, Roure F, Peköz T. An experimental investigation of distortional buckling of steel storage rack columns. Thin-Walled Structures. 2011;49(8)：933-46.

[19] Dos Santos ES, Batista EM, Camotim D. Experimental investigation concerning lipped channel columns undergoing local – distortional – global buckling mode interaction. Thin-Walled

Structures. 2012;54：19-34.

[20] Niu S, Rasmussen KJR, Fan F. Distortional－global interaction buckling of stainless steel Cbeams: Part I-Experimental investigation. Journal of Constructional Steel Research. 2014;96：127-39.

[21] Landesmann A, Camotim D, Garcia R. On the strength and DSM design of cold-formed steel web/flange-stiffened lipped channel columns buckling and failing in distortional modes. Thin-Walled Structures. 2016;105：248-65.

[22] Haidarali MR, Nethercot DA. Local and distortional buckling of cold-formed steel beams with both edge and intermediate stiffeners in their compression flanges. Thin-Walled Structures. 2012;54：106-12.

[23] Niu S, Rasmussen KJR, Fan F. Distortional－global interaction buckling of stainless steel C-beams: Part II—Numerical study and design. Journal of Constructional Steel Research. 2014;96：40-53.

[24] Ren C, Zhao X, Chen Y. Buckling behaviour of partially restrained cold-formed steel zed purlins subjected to transverse distributed uplift loading. Engineering Structures. 2016;114：14-24.

[25] Liu Q, Yang J, Chan AHC, Li LY. Pseudo-plastic moment resistance of continuous beams with cold-formed sigma sections at internal supports: A numerical study. Thin-Walled Structures. 2011;49(12)：1592-604.

[26] Valsov VZ. Thin-walled elastic beams. Jerusalem, Israel: Israel Program for Scientific Translations, 1961.

[27] Timoshenko SP, Gere JM. Theory of elastic stability: McGraw-Hill, 1936.

[28] Chawalit M, Eiichi W, Tomoaki U. Shear buckling of corrugated plates with edges elastically restrained against rotation. International Journal of Structural Stability and Dynamics. 2004;4(1)：89-104.

[29] Easley JT, McFarland DE. Buckling of light-gage corrugated metal shear diaphragms. Journal of the Structural Division. 1969;95(7)：1497-516.

[30] Ajeesh SS, Arul Jayachandran S. Simplified semi-analytical model for elastic distortional buckling prediction of cold-formed steel flexural members. Thin-Walled Structures. 2016;106：420-7.

[31] Zhao CX, Yang J, Wang FL, Chan AHC. Rotational stiffness of cold-formed steel roof purlin－sheeting connections. Engineering Structures. 2014;59：284-97.

[32] Schafer BW. CUFSM4.05 — finite strip buckling analysis of thin-walled members. Baltimore,U.S.A.: Department of Civil Engineering, Johns Hopkins University, http://www.ce.jhu.edu/bschafer/cufsm/. 2012.

[33] Albion Sections Ltd Albion sections Sigma purlin technical manual. Birmingham, UK http://www.albionsections.co.uk. 2008.

Graphic Abstract